THE 1/5 LAW FOR CHAOS IN THE THREE-BODY PROBLEM AT MODERATE ECCENTRICITY

Christopher Culter[1]

cculter@berkeley.edu

ABSTRACT

In this paper, we generalize Wisdom's 2/7 law to the case of finite eccentricity. We consider the restricted, planar, circular three-body problem. If μ is the secondary mass, e is the particle eccentricity, and x is the particle-to-secondary separation, the 2/7 law states that chaos ensues if $e = 0$ and $x < \mu^{2/7}$. Our law states that any nonresonant orbit with either $x < \mu^{1/7}$ or $x < (e\mu)^{1/5}$ is chaotic; we call the latter condition the "1/5 law." We present analytic arguments for the 1/5 law, and we successfully test it with a variety of numerical experiments.

Subject headings: celestial mechanics — instabilities — methods: numerical — minor planets, asteroids

1. INTRODUCTION

Chaos is ubiquitous in celestial mechanics. In the solar system, chaotic interactions with the planets shape the structure of the minor bodies, including the asteroid belt and the Kuiper belt (Lecar 2001). In particular, the outer edge of the asteroid belt is known to occur at the semi-major axis where first-order mean-motion resonances with Jupiter overlap, giving rise to chaos. The actual mechanisms by which Jupiter depletes some regions of asteroids include three-body secular resonances with Saturn and the ejection of eccentric particles by Mars. Nonetheless, we can understand the location of the belt's outer edge by analyzing a simplified problem in which the perturbing planet executes a circular orbit about the sun, and there are no other planets. In this paper, we consider the restricted, planar, circular three-body problem.

Let μ be the secondary-to-primary mass ratio and x the separation between the orbits of the secondary and a test particle. Wisdom's (1980) 2/7 law states that for zero particle

[1]UC Berkeley Physics Department

eccentricity, the value of x which separates chaotic and regular behavior scales as $\mu^{2/7}$. Duncan et al. (1989) remark that the condition $x < \mu^{2/7}$ is also sufficient to produce chaos at finite eccentricity, although it is no longer necessary. We derive a necessary and sufficient condition by removing the assumption of zero eccentricity and applying analytic arguments similar to those in (Wisdom 1980) and (Duncan et al. 1989). Our new condition generalizes the 2/7 law to finite eccentricity e. At sufficiently large e, the new condition predicts the boundary between chaotic and regular behavior to scale as $x \sim (e\mu)^{1/5}$. We call this result the 1/5 law.

We find that the encounter mapping used successfully by Duncan et al. (1989) to test the 2/7 law is insufficient to test the 1/5 law. Instead, we perform numerical experiments using the encounter maps described by Namouni et al. (1999); these maps can be made accurate to arbitrarily high order in e. Experiments using the order 2 map and the order 10 map confirm both the 2/7 law and the 1/5 law.

2. ANALYTIC CONSIDERATIONS

In this section we more precisely define the variables of our system. We determine the scaling laws of the dominant interactions: in particular, the change in the particle's eccentricity due to a single encounter is $\sim \mu/x^2$. From this relation, we obtain an analytic criterion for the onset of chaos. We define an indicator variable Z containing a μ^2/x^7 term and an $e\mu/x^5$ term; if $Z \ll 1$ then the motion is regular, and if $Z \gg 1$, the motion is either stably resonant or chaotic. At moderate eccentricity the second term dominates Z, so the boundary between regular and chaotic behavior is found at $x \sim (e\mu)^{1/5}$. This is the 1/5 law.

We employ an impulse approximation to determine the changes to the particle's eccentricity. From conservation of the Jacobi constant we then deduce the behavior of the separation x and the longitudes of conjunction λ. The indicator Z is motivated by two criteria for chaos: resonance overlap and the decay of correlations in the history of λ.

2.1. Impulse Approximation

The system comprises a primary mass m_1, a secondary mass m_2 in a circular orbit about m_1, and a massless test particle in the plane of m_1 and m_2. We require that $m_2 \ll m_1$ and that the test particle reside between the orbits of m_1 and m_2.

The total mass m_1+m_2, the gravitational constant, and the distance between m_1 and m_2 are all normalized to unity. Let $\mu = m_2/(m_1+m_2) \ll 1$ and let a, e, and $\tilde{\omega}$ be the barycentric

semimajor axis, eccentricity, and longitude of periapse of the test particle, respectively. Define the separation $x = 1 - a$ and the eccentricity vector $\boldsymbol{e} = (e\cos\tilde{\omega})\hat{\boldsymbol{x}} + (e\sin\tilde{\omega})\hat{\boldsymbol{y}}$. We focus on the case when the test particle is far from the Hill sphere, so that $\mu^{1/3} \ll x \ll 1$. Additionally, in the absence of mean-motion resonances, we must have $e < x$ to prevent orbit crossing. We treat μ and e/x as small parameters in our Taylor expansions.

We approximate the motion of the particle by a Keplerian orbit around m_1 interrupted by a series of instantaneous impulses during conjunctions with m_2. Between conjunctions, $x, \boldsymbol{e}$, and the mean motion $n = (1-x)^{-3/2}$ are taken to be constant. Since the mean motion of m_2 is unity, the time T between successive conjunctions ("synodic period") is

$$\begin{aligned} T &= \frac{2\pi}{(1-x)^{-3/2} - 1} && (1)\\ &= \frac{4\pi}{3x + \mathcal{O}(x^2)} && (2)\\ &= \frac{4\pi}{3x} + \mathcal{O}(1). && (3) \end{aligned}$$

We define λ as the longitude at a conjunction and $\Delta\lambda$ as the difference in longitudes of conjunction between successive conjunctions. During time T, m_2 passes through T radians; then

$$\Delta\lambda = T \pmod{2\pi}. \tag{4}$$

To calculate the change in x and $\boldsymbol{e}$ during a conjunction we use an encounter map as described in the next section. For now, we estimate the change in $\boldsymbol{e}$ to lowest order in μ and e/x by using the identity

$$\boldsymbol{e} = \boldsymbol{v} \times (\boldsymbol{r} \times \boldsymbol{v}) - \hat{\boldsymbol{r}}, \tag{5}$$

where $\boldsymbol{r}, \boldsymbol{v}$ are the inertial-frame position and velocity vectors of the test particle. To first order,

$$\delta\boldsymbol{e} \approx \delta\boldsymbol{v} \times (\boldsymbol{r} \times \boldsymbol{v}) + \boldsymbol{v} \times (\delta\boldsymbol{r} \times \boldsymbol{v}) + \boldsymbol{v} \times (\boldsymbol{r} \times \delta\boldsymbol{v}) - \delta\hat{\boldsymbol{r}}. \tag{6}$$

Let s be the distance between the test particle and m_2, u be the relative velocity between the test particle and m_2, and $\boldsymbol{F}$ be the force on the test particle exerted by m_2. We write $s_0, u_0, \boldsymbol{F}_0$ for the values of $s, u, \boldsymbol{F}$ at conjunction:

$$\begin{aligned} s_0 &= x + \mathcal{O}(e), && (7)\\ u_0 &= n - 1 + \mathcal{O}(e) && (8)\\ &= 3x/2 + \mathcal{O}(x^2) + \mathcal{O}(e), && (9)\\ \boldsymbol{F}_0 &= \frac{\mu}{s_0^2}\hat{\boldsymbol{r}} && (10)\\ &= \frac{\mu}{x^2}\hat{\boldsymbol{r}}\left[1 + \mathcal{O}(e/x)\right]. && (11) \end{aligned}$$

Let τ be the period of time during which $s \sim s_0$; then

$$\tau \sim \frac{s_0}{u_0} = \frac{2}{3} + \mathcal{O}(x) + \mathcal{O}(e/x). \tag{12}$$

The impulse is

$$\begin{aligned} \delta \boldsymbol{v} &= \int \boldsymbol{F}\, dt & (13)\\ &\sim \tau \boldsymbol{F}_0 + \mathcal{O}\left(\tau^3 \frac{d^2\boldsymbol{F}}{dt^2}\right). & (14) \end{aligned}$$

To lowest order in x and e/x, $d^2\boldsymbol{F}/dt^2$ vanishes, and we are left with

$$\delta \boldsymbol{v} \sim \frac{\mu}{x^2}\hat{\boldsymbol{r}}. \tag{15}$$

Since $\delta \boldsymbol{v}$ is directed along $\boldsymbol{r}$, $\boldsymbol{r} \times \delta \boldsymbol{v}$ vanishes; and since we are working in the impulse approximation, $\delta \boldsymbol{r}$ also vanishes. Equation (6) reduces to its first term:

$$\begin{aligned} \delta \boldsymbol{e} &\approx \delta \boldsymbol{v} \times \hat{\boldsymbol{z}} & (16)\\ &\sim -\frac{\mu}{x^2}\hat{\boldsymbol{\theta}}. & (17) \end{aligned}$$

We also want to determine δx. The above expression for $\delta \boldsymbol{e}$ is accurate to first order in μ and zeroth order in e/x. However, to these orders, $\delta x \approx 0$. Rather than explicitly include $\mathcal{O}(\mu^2)$ terms in the above analysis, we employ a trick that exploits the conservation of the Jacobi constant. Expanding the Jacobi constant to lowest order in x and e, the combination $3x^2 - 4e^2$ is conserved; see Murray & Dermott (1999) eq. (3.213) for a derivation based on Tisserand's relation. Assuming for the moment that $\delta x \ll x$ we get

$$2x\delta x \approx \frac{4}{3}\left(|\delta \boldsymbol{e}|^2 + 2\boldsymbol{e}\cdot\delta \boldsymbol{e}\right). \tag{18}$$

Combining eqs. (3) and (18), we find the change in synodic period due to a single kick:

$$\begin{aligned} \delta T &\approx \frac{4\pi}{3x^2}\delta x & (19)\\ &\approx \frac{8\pi}{9x^3}(|\delta \boldsymbol{e}|^2 + 2\boldsymbol{e}\cdot\delta \boldsymbol{e}) & (20)\\ &\sim \frac{8\pi}{9x^3}\left[\frac{\mu^2}{x^4} + \frac{2e\mu}{x^2}\sin(\lambda - \tilde{\omega})\right] & (21)\\ &\sim \frac{8\pi\mu^2}{9x^7} + \frac{16\pi e\mu}{9x^5}\sin(\lambda - \tilde{\omega}). & (22) \end{aligned}$$

We call $\delta\Delta\lambda$ the change in $\Delta\lambda$ after a conjunction: $\delta\Delta\lambda = \delta T$.

2.2. Criteria for Chaos

Generally, we should expect chaos to appear in a dynamical system when resonances overlap (Chirikov 1979, Lecar et al. 2001). Since $e \ll 1$, in our system the first-order mean-motion resonances are the most important. In a first-order resonance λ is constant; every first-order resonance is characterized by an integer m such that $\Delta\lambda = 2\pi m$. For a particle to inhabit the overlap between two neighboring resonances m and $m \pm 1$, it must be able to jump from m to $m \pm 1$ within a single conjunction. This requirement translates to the condition

$$|\delta T| = |\delta\Delta\lambda| \geq 2\pi. \tag{23}$$

We therefore expect an orbit to be chaotic if $|\delta T|$ ever attains order unity. If an orbit is not protected by a single mean-motion resonance, then regardless of chaos the angle $\lambda - \tilde{\omega}$ should sample all values. Since we are interested in the largest δT an orbit suffers during its conjunctions, if an orbit is non-resonant then we may replace Eq. (22) with the indicator

$$Z = \frac{8\pi}{9}\left(\frac{\mu^2}{x^7} + \frac{2e\mu}{x^5}\right). \tag{24}$$

If $Z \gg 1$ then the orbit is either resonant or chaotic; if $Z \ll 1$ then the orbit is regular.

We can also motivate the indicator Z through a heuristic argument made by Duncan et al. (1989) which does not explicitly rely on mean-motion resonances. If μ were zero then $\delta\Delta\lambda$ would vanish; the longitudes of conjunction would circulate at a constant rate. Instead, $\delta\Delta\lambda$ measures the perturbation in the longitudes of conjunction; if the perturbation is ever too great, say $> \pi$, then the sequence of longitudes "forgets" its past behavior and chaos ensues. Duncan et al. (1989) include only the μ^2/x^7 term in $\delta\Delta\lambda$, but we can adapt their argument to our more accurate expression. Taking the maximum of $\delta\Delta\lambda$ as $\lambda - \tilde{\omega}$ samples all values, we again derive the indicator Z in eq. (24).

Note that neither argument for the indicator Z predicts the exact threshold value between ordered and chaotic behavior; we must determine the threshold experimentally.

2.3. The 1/5 Law

Due to the presence of protective mean-motion resonances, the condition $Z \gg 1$ is necessary but not sufficient to produce chaos. Nonetheless, when $Z \sim 1$, first-order mean-motion resonances do not cover the entire phase space, so we should be able to find at least a few chaotic orbits with Z just greater than order unity. For given initial conditions $\boldsymbol{e}, \tilde{\omega}$, and λ, let us define x^* to be the largest x for which the motion is chaotic. By the argument just given, we expect $Z(x^*) \sim 1$.

If the eccentricity is small, $e \ll \mu/x^2$, then Z is dominated by its first term. In this case we have

$$Z(x^*) \sim \frac{\mu^2}{(x^*)^7} \sim 1 \tag{25}$$

and therefore

$$x^* \sim \mu^{2/7}. \tag{26}$$

Equation (26) is Wisdom's (1980) "2/7 law" for the onset of chaos. On the other hand, if the eccentricity is large compared with that induced by an individual kick—that is, if $e \gg \mu/x^2$—then Z is dominated by its second term. In this case we have

$$Z(x^*) \sim \frac{e\mu}{(x^*)^5} \sim 1 \tag{27}$$

and therefore

$$x^* \sim (e\mu)^{1/5}. \tag{28}$$

The "1/5 law" for chaos at moderate eccentricity is a new result.

3. NUMERICAL EXPERIMENTS

3.1. Maps

Let $\boldsymbol{e}_n, x_n$, and λ_n be the values of $\boldsymbol{e}, x$, and λ immediately preceding the nth conjunction. A numerical procedure which takes as its input $(\boldsymbol{e}_n, x_n, \lambda_n)$ and outputs $(\boldsymbol{e}_{n+1}, x_{n+1}, \lambda_{n+1})$ is called an *encounter map*. Encounter maps approximate the true motion, and some are more accurate than others.

Duncan et al. (1989) use eq. (17) to define an encounter map, hereafter the "DQT map." Its derivation assumes $e \ll \mu/x^2$. By contrast, we are primarily interested in the $e \gg \mu/x^2$ regime. Namouni et al. (1996) describe a family of more accurate encounter maps that expand the interaction Hamiltonian in $\boldsymbol{e}/x$ to arbitrary order. The "order M Namouni map" employs a Fourier expansion in $(\lambda - \tilde{\omega})$ up to order M, followed by a Taylor expansion in e up to order M. We implement Namouni maps of orders $1, 2$, and 10. Below, we present the order 2 map in detail, after which we define the maps of orders 1 and 10 through modifications of the order 2 map.

To begin computing the second order Namouni map, we define an intermediate eccentricity vector $\boldsymbol{e}'_n$ that reflects the first-order shift in $\boldsymbol{e}$,

$$\boldsymbol{e}'_n = \boldsymbol{e}_n - g\frac{\mu}{x_1^2}\hat{\boldsymbol{\theta}}, \tag{29}$$

where the interaction strength

$$g = \frac{16}{9} K_0\left(\frac{2}{3}\right) + \frac{8}{9} K_1\left(\frac{2}{3}\right) \approx 2.239567,$$

and K_0, K_1 are modified Bessel functions of the second kind. The value of g is given as an elliptic integral in Appendix B of Namouni et al. (1996); it also appears in eq. (9) of Duncan et al. (1989). In rectangular coordinates, eq. (29) becomes

$$e'_{nx} = e_{nx} + g\frac{\mu}{x_1^2}\sin\lambda_n, \tag{30}$$

$$e'_{ny} = e_{ny} - g\frac{\mu}{x_1^2}\cos\lambda_n. \tag{31}$$

We then define $\boldsymbol{e}_{n+1}$ as a higher-order correction to $\boldsymbol{e}$. In polar $e, \tilde{\omega}$ coordinates, we have

$$e_{n+1}^2 = e_n'^2 + 4g_2\sin(2\lambda_n - 2\tilde{\omega}'_n)\,\frac{\mu}{x_1^3}\,e_{n+1}^2, \tag{32}$$

$$\tilde{\omega}_{n+1} = \tilde{\omega}'_n + \left(\frac{2}{3} + g_2\cos(2\lambda_n - 2\tilde{\omega}'_n)\right)\frac{\mu}{x_1^3}, \tag{33}$$

where

$$g_2 = \frac{160}{27} K_0\left(\frac{4}{3}\right) + \frac{152}{27} K_1\left(\frac{4}{3}\right) \approx 3.571554.$$

In the notation of Namouni et al. (1996), $g_2 = -(4/3)W_2^{2,0}$. We determine x_{n+1} by conservation of the Jacobi constant:

$$x_{n+1}^2 = x_n^2 + \frac{4}{3}(e_{n+1}^2 - e_n^2). \tag{34}$$

Finally, we use the new separation x_{n+1} to get the longitude λ_{n+1} of the next conjunction:

$$\lambda_{n+1} = \lambda_n + \frac{4\pi}{3x_{n+1}}. \tag{35}$$

Equations (29)–(35) correspond to equations (36)–(43) in Namouni et al. (1996). Their equations look superficially different from ours because their variables suppress factors of $\mu/3$. Furthermore, Namouni et al.'s eqs. (37) and (38) contain typographical errors: $\sin\lambda_n$ and $\cos\lambda_n$ should be exchanged for one another. Note that the map employs the initial separation x_1 instead of the current separation x_n; this change ensures the symplecticness of the map without altering its qualitative behavior (Namouni et al. 1996, Duncan et al. 1989).

It is straightforward to generalize the above order 2 map to obtain encounter maps of other orders. Equations (30), (31), (34), and (35) apply to all the Namouni maps. The order 10 map extends eqs. (32) and (33) into degree 10 and degree 8 polynomials in e_{n+1},

respectively. Equation (32) is then solved for e_{n+1} implicitly, using the modified Newton-Raphson scheme described in eq. (2.62) of Murray & Dermott (1999).

The order 1 Namouni map replaces eqs. (32) and (33) with $\boldsymbol{e}_{n+1} = \boldsymbol{e}'_n$. This map is almost, but not precisely, the DQT map, which uses eq. (1) to advance λ. In other words, DQT replaces eq. (35) with $\lambda_{n+1} = \lambda_n + 2\pi/[(1-x)^{-3/2} - 1]$.

3.2. Experimental Setup

We design two types of experiments that use the Namouni encounter maps to test the validity of the 2/7 and 1/5 laws. First, we attach a tangent map to the encounter map, allowing us to directly test for chaos by estimating Lyapunov exponenents. Such tests are most useful for broadly characterizing the chaotic zone in phase space. Second, to precisely measure the outer limit of the chaotic zone, we develop a simpler criterion for instability. We define a stepping algorithm that applies the new criterion to home in on the boundary of chaos.

The indicator Z which we intend to test is a function of x and e but not of $\tilde{\omega}$ or λ. We must therefore decide which initial angles $\tilde{\omega}_1$ and λ_1 we should choose in our experiments. When an orbit resides in a single first-order interior mean-motion resonance—in fact, any interior resonance of odd order (Murray & Dermott 1999)—the angle $\lambda - \tilde{\omega}$ librates about 0. It follows that orbits with $\lambda_1 - \tilde{\omega}_1 = \pi$ are least likely to be protected by resonances. Since our experiments are meant to find x^* and not to map out the resonant islands below x^*, we set $\lambda_1 = 0$ and $\tilde{\omega}_1 = \pi$ in all the following experiments.

3.2.1. Criterion 1: The tangent map

Chaos in a dynamical system is characterized by exponential separation of infinitesimally close orbits. For any map, one can test for chaos by calculating two nearby orbits, a "particle" and its "shadow," and measuring their separation rate. This method requires us to periodically rescale the separation to ensure that the shadow remain close to the particle; yet if they get too close, we suffer from numerical round-off errors. Fortunately, the encounter map is simple enough that we can use the *tangent map* method instead.

The tangent map runs in parallel with the encounter map; it calculates the orbit of a shadow whose separation from the particle is a true infinitesimal $(d\boldsymbol{e}, dx, d\lambda)$. We choose $dx_1 = 0$. The tangent map equations are the total derivatives of the encounter map equations;

for example, eq. (30) implies

$$de'_{nx} = de_{nx} + g\frac{\mu}{x_1^2}(\cos\lambda_n)d\lambda_n. \tag{36}$$

The Lyapunov exponent is

$$\ell = \lim_{n\to\infty} \frac{\ln|d\boldsymbol{e}_n|}{n}; \tag{37}$$

if $\ell > 0$ then the orbit is chaotic by definition. Of course, we cannot take the limit $n \to \infty$ numerically. We are most interested in the boundary between chaotic and regular behavior, and ℓ converges very slowly as we approach this boundary. Nonetheless we can use the Lyapunov exponent to broadly map out the regimes which are definitely regular or chaotic.

3.2.2. Criterion 2: Eccentricity growth

To more precisely determine the outer boundary of chaos, we apply a simple observational criterion for instability (Duncan et al. 1989). In a chaotic orbit, the eccentricity vector executes a random walk, and eventually it develops $e > x_1$. Therefore we label an orbit *stable* if during the length of a computation we always have $e < x_1$; if any e_n ever surpasses x_1 then we label the orbit *unstable* and halt the calculation.

Due to conservation of the Jacobi constant, as e grows larger than e_1, so x must grow larger than x_1. Therefore our condition $e_n > x_1$ for instability does not imply the orbit-crossing condition $e_n > x_n$; neither does it imply that the particle will enter the Hill sphere or be ejected from the system. The new instability condition is therefore sensitive to bounded chaos.

Given e_1 and μ, we wish to find the maximum unstable x_1, which we call x^* as before. Duncan et al. (1989) use a recursive bisection algorithm: they pick an interval $[X_1, X_2]$ believed to contain x^* and test the midpoint orbit $x_1 = (X_1 + X_2)/2$. If x_1 is stable, the algorithm sets $X_2 := x_1$; otherwise it sets $X_1 := x_1$. Once the interval shrinks to some desired accuracy, the algorithm reports that it has found x^*. This method works for the DQT map, but it relies on the assumption that the space of regular orbits is connected; so if x_1 is regular then all of $[x_1, \infty)$ is regular. As Namouni et al. point out, the phase space of the DQT map is unrealistic. We find that the bisection algorithm does not reliably find x^* for the higher-order Namouni maps; instead it often gets "caught" near islands of stability which can be found anywhere between x^* and the Hill sphere. Figure 1 illustrates the phenomenon with the order 10 map. This error reflects a deficiency in the bisection algorithm, not the encounter map.

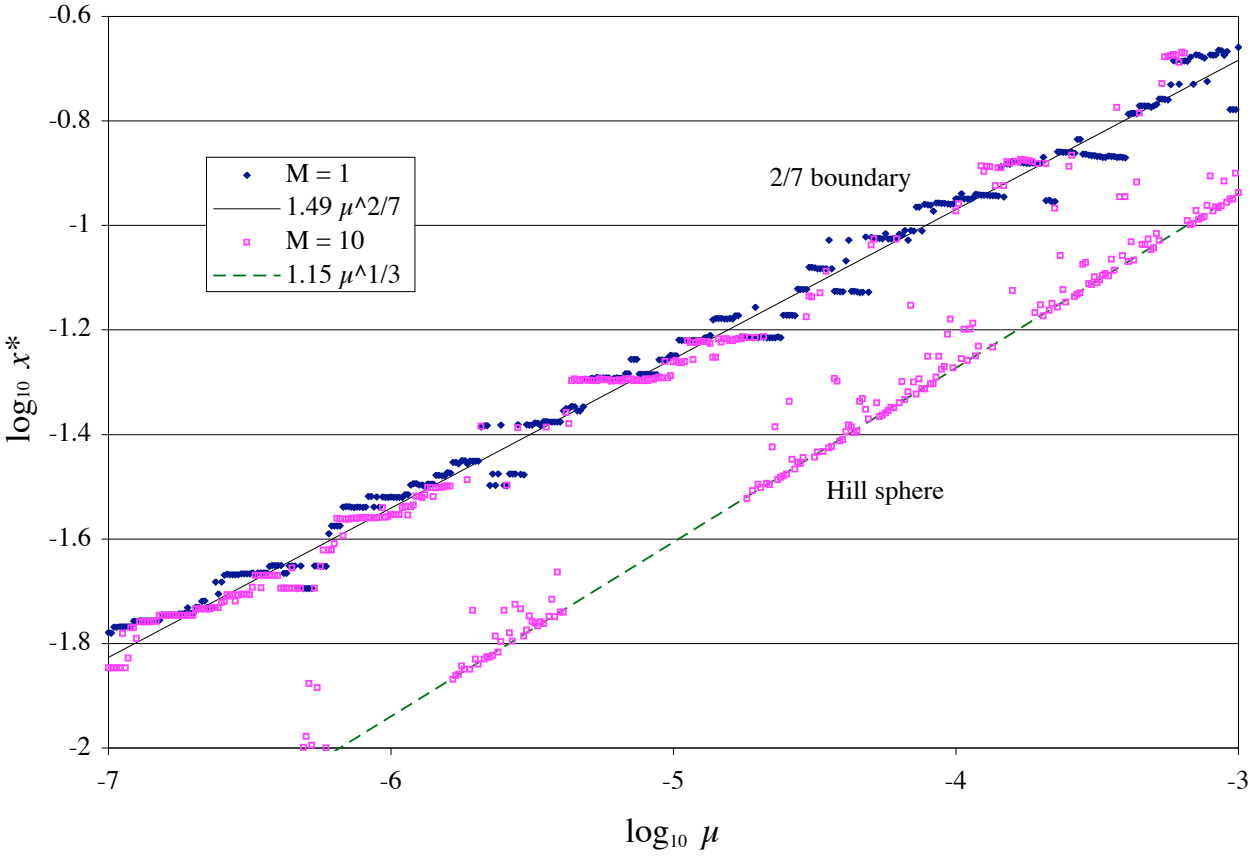

Fig. 1.— Analogue to Figure 2 of Duncan et al. (1989), using order 1 and 10 Namouni maps. The bisection algorithm determines x^*; the experimental parameters are $e_1 = 0, N = 10^3$; the stability criterion is $e < x_1$. We also plot the 2/7 law and the Hill sphere.

To find x^* with our higher-order maps, we employ a stepping algorithm which starts in the stable region and gingerly steps downward to find the largest unstable orbit in its path. We pick an x_1 believed to be greater than x^* and a step size D, and we test the orbit x_1. If x_1 is stable, we assign $x_1 := x_1 - D$. Otherwise, we assign $x_1 := x_1 + 3D$ and $D := D/4$; the algorithm retreats well back into the supposedly stable region and resumes stepping down more slowly. When D reaches the desired accuracy, we conclude $x^* = x_1 \pm D$. The stepping algorithm is much slower than the bisection algorithm, but it finds x^* more reliably.

Like Duncan et al. (1989), we calculate the midpoint $x_1 = (X_1 + X_2)/2$ and the step $x_1 := x_1 + 3D$ in logarithmic units. Therefore the bisections are evenly spaced on the logarithmic vertical axis of Figure 1.

3.3. Results

3.3.1. Criterion 1: The tangent map

We calculated a grid of orbits of the order 10 Namouni map + tangent map with μ ranging from 10^{-25} to 10^{-5}, $e_1 = 0$, and Z ranging from 0.0001 to 100. The results are graphed in Fig. 2. A similar experiment was carried out in which $e_1 = 2\mu^{1/3}$; those results are in Fig. 3. Since particles outside the Hill sphere have $x_1 > \mu^{1/3}$, every orbit of this latter experiment has $e_1 > 2\mu/x_1^2$. Thus the condition $e_1 = 2\mu^{1/3}$ insures that the 1/5 law applies.

The experiments support the indicator hypothesis: for nonresonant orbits, $Z \ll 1$ implies regularity and $Z \gg 1$ implies chaos. We also carried out experiments with $e_1 = 0.5\mu, \mu$, and 5μ; the resulting data do not contain any new features, and they continue to support our interpretation of Z.

3.3.2. Criterion 2: Eccentricity growth

We used the stepping algorithm with the order 10 Namouni map to find x^* for μ between 10^{-18} and 10^{-2}, and fixed $e_1 = 10^{-4}$; the results are displayed in Figure 4. Series of experiments are run having different values of the maximum iteration N. For $\mu > 10^{-12}$, $N = 5 \times 10^4$ is sufficient to converge on x^*, while for $10^{-18} < \mu < 10^{-12}$, $N = 2 \times 10^6$ suffices. There are three regimes of interest. For $\mu > 10^{-12}$, we have $e_1 \ll \mu/(x^*)^2$. The data in this regime follow Wisdom's 2/7 law,

$$x^* = A\mu^{2/7}.$$

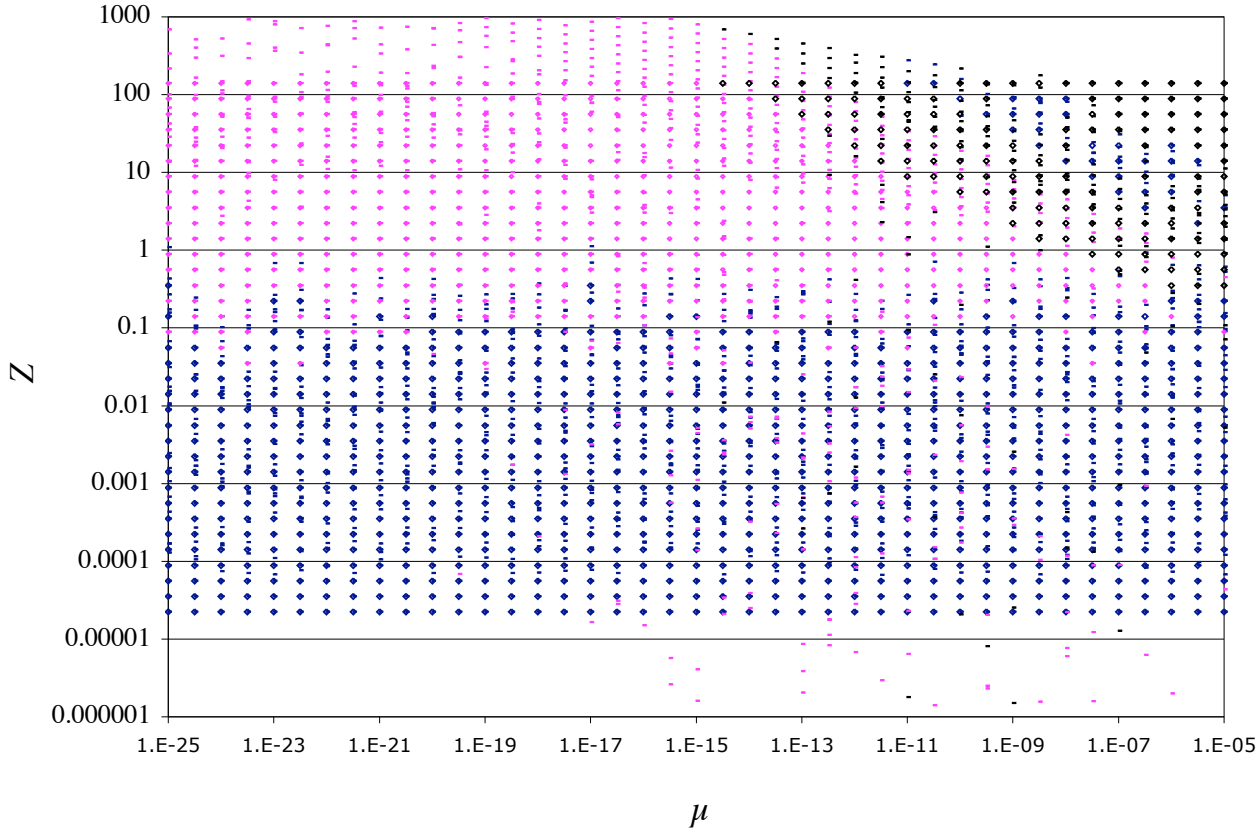

Fig. 2.— Chaotic boundary of the order 10 Namouni map + tangent map as determined by Lyapunov exponents. Every orbit has $e_1 = 0$. Regular orbits are plotted as blue points; chaotic orbits are plotted as magenta points. Orbits which hit the Hill sphere and were ejected are shown in black. Each point is followed up to 32000 conjunctions.

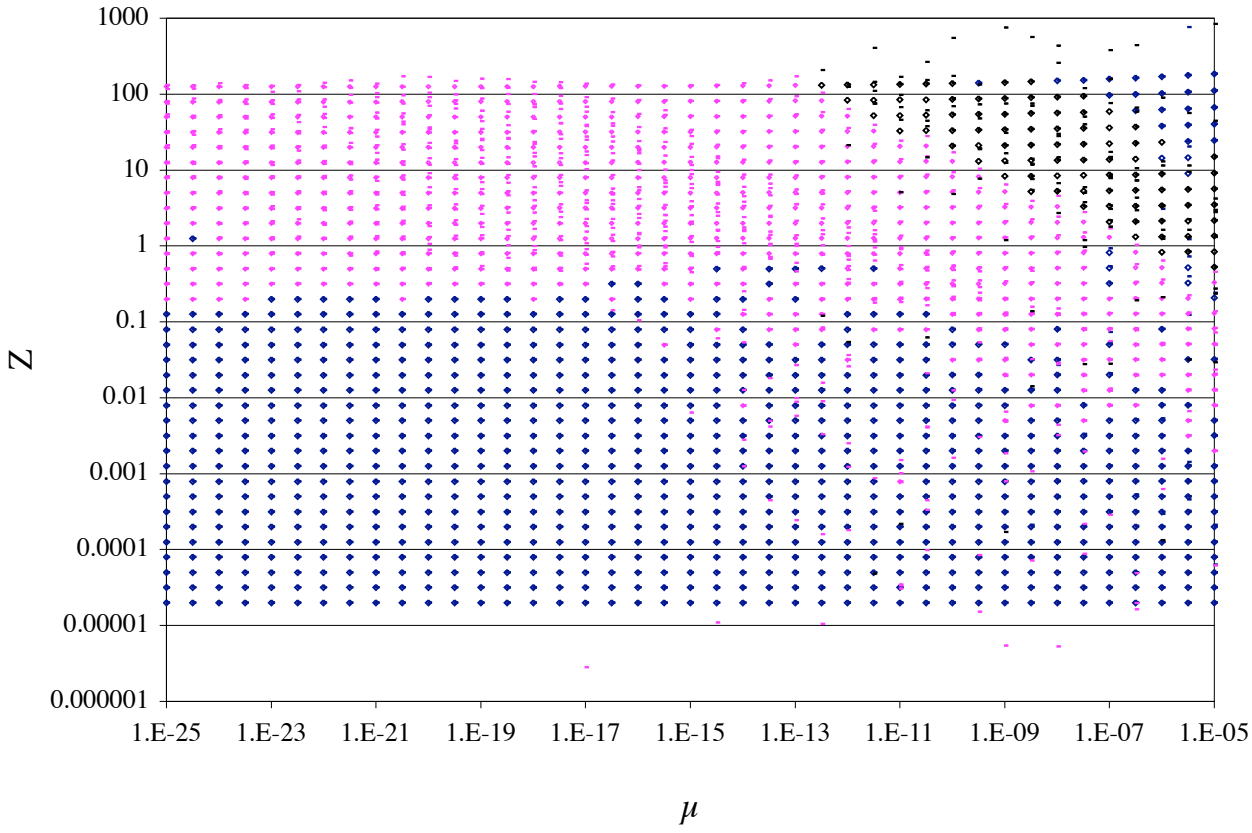

Fig. 3.— The same experiment as in Fig. 2, except that every orbit here has $e_1 = 2\mu^{1/3}$.

For $10^{-18} < \mu < 10^{-12}$, $e_1 \gg \mu/(x^*)^2$. Here, the data follow our 1/5 law,

$$x^* = B(e\mu)^{1/5}.$$

Finally, for $\mu < 10^{-18}$ we have $x^* = e$, since if $x_1 < e$ then the orbit is immediately tagged as unstable.

We fit values of A and B to the data; the result is the modified indicator

$$Z' = 45\frac{\mu^2}{x^7} + 10\frac{e\mu}{x^5}. \tag{38}$$

In Figure 4 and all the figures to follow, the solid line represents the prediction of x^* based on the condition $Z'(x^*) = 1$, where Z' is given by eq. (38).

We repeated the experiment represented by Figure 4 with the order 2 Namouni map; the results are displayed in Figure 5. Since the order 2 map is faster to compute, we were able to run it for longer N and verify that x^* has converged at all masses. The same modified indicator Z' is plotted, demonstrating that the order 2 map and the order 10 map agree for our purposes.

We also reversed the roles of e_1 and μ in an experiment plotting x^* against e_1 in which $\mu = 10^{-12}$ is held fixed. Those results are displayed in Figure 6. The physical regimes are now encountered in reverse order; the horizontal line on the left side of Figure 6 reflects the 2/7 law, while the right side reflects the degenerate $x^* = e_1$ case. The middle regime is again the 1/5 law.

Finally, we repeated the experiment represented by Figure 4 with the order 1 Namouni map; the results are displayed in Figure 7. Here we see several changes in behavior from the order 2 map; the order 1 map seems to adhere to a 2/7 law at high μ, but the value of x^* is higher than before. More strikingly, the 1/5 law never appears.

4. CONCLUSIONS

In this work, we generalize Wisdom's (1980) 2/7 law to finite eccentricity. Our new law can be motivated by considering either overlap of first-order mean-motion resonances or the requirement that the longitudes of conjunction lose long-term correlations. For $e \gg \mu/x^2$, the boundary value of x between chaotic and regular behavior no longer scales as $\mu^{2/7}$ but as $(e\mu)^{1/5}$. We test the new prediction with a combination of numerical techniques drawn from Duncan et al. (1989) and Namouni et al. (1996). All but one of our experiments confirm both the 2/7 and 1/5 laws; only the least accurate encounter map disagrees.

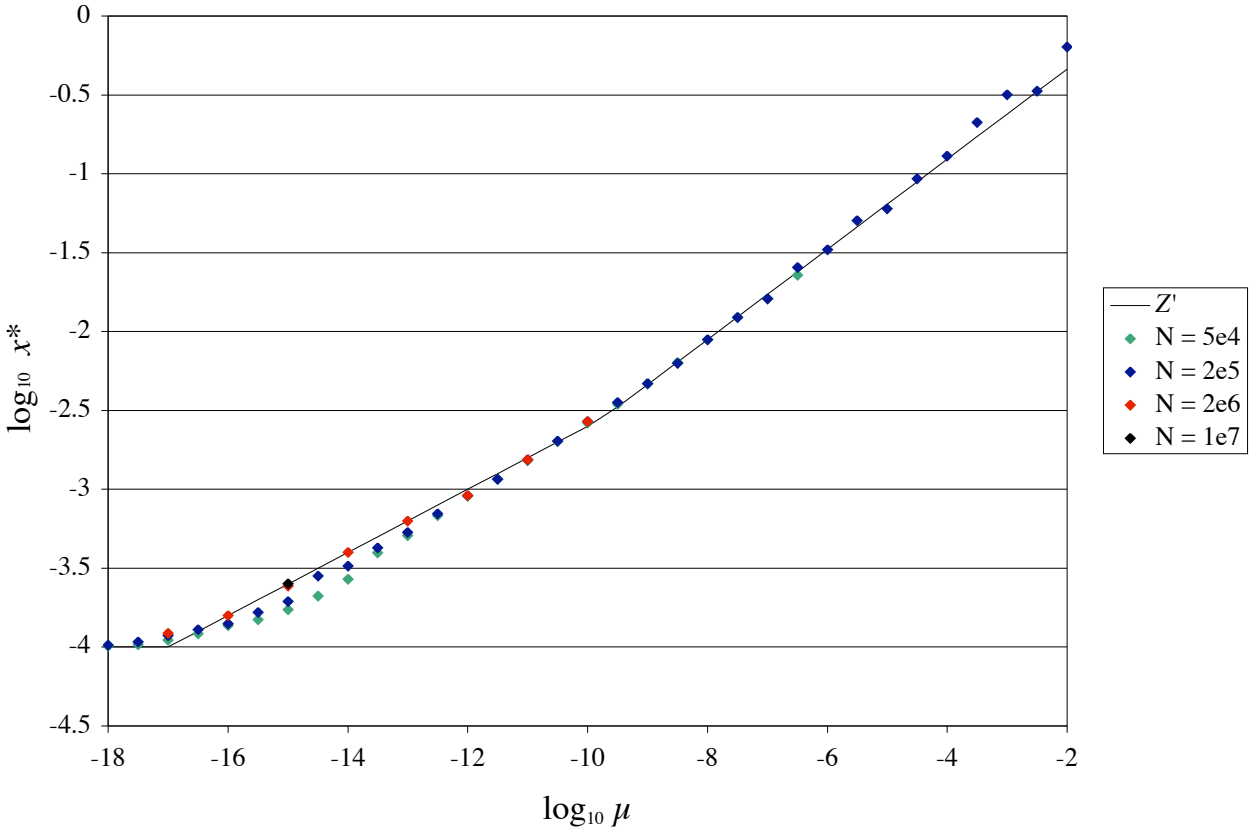

Fig. 4.— Plot of x^* versus μ, given fixed $e_1 = 10^{-4}$; the order 10 Namouni map is applied up to 10^7 times; the stability criterion is $e < x_1$. The prediction of the modified indicator Z' is plotted for comparison.

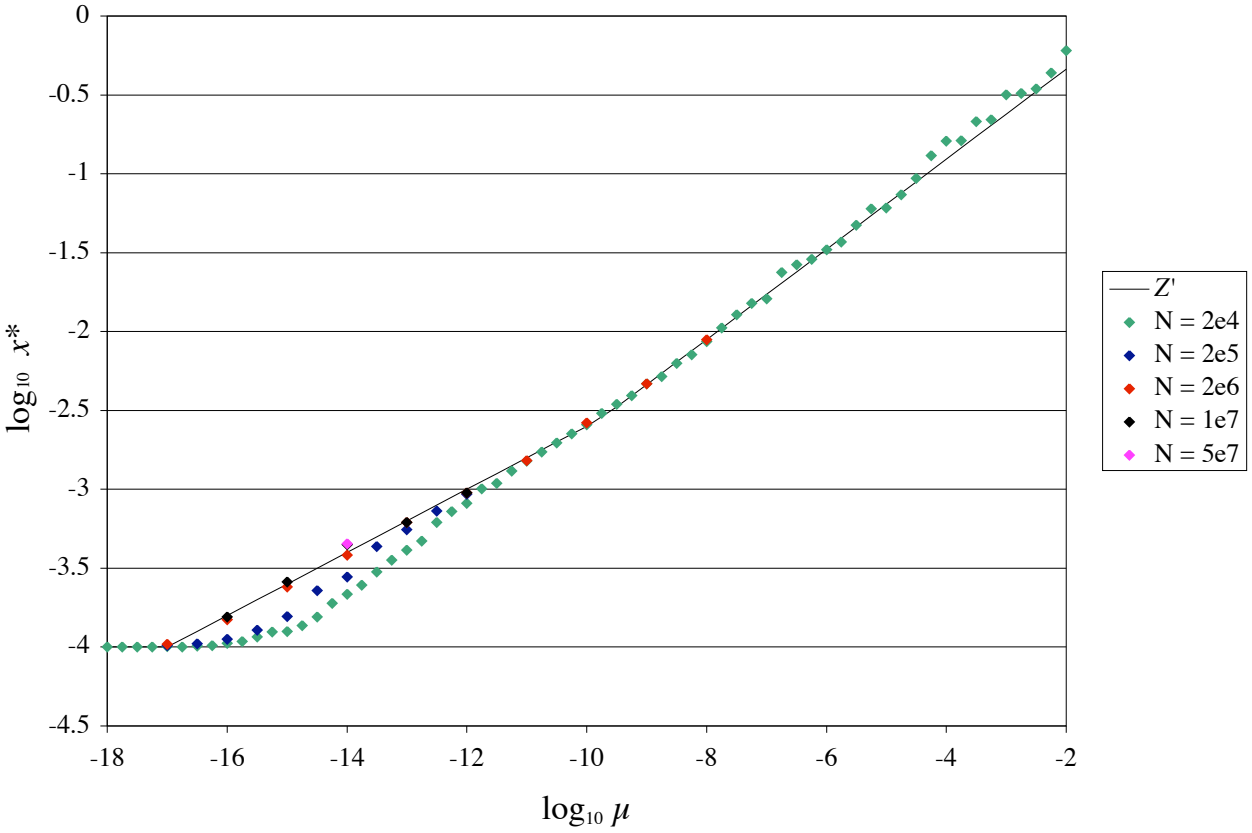

Fig. 5.— Plot of x^* versus μ, given fixed $e_1 = 10^{-4}$; the order 2 Namouni map is applied up to 5×10^7 times; the stability criterion is $e < x_1$. The prediction of the modified indicator Z' is plotted for comparison.

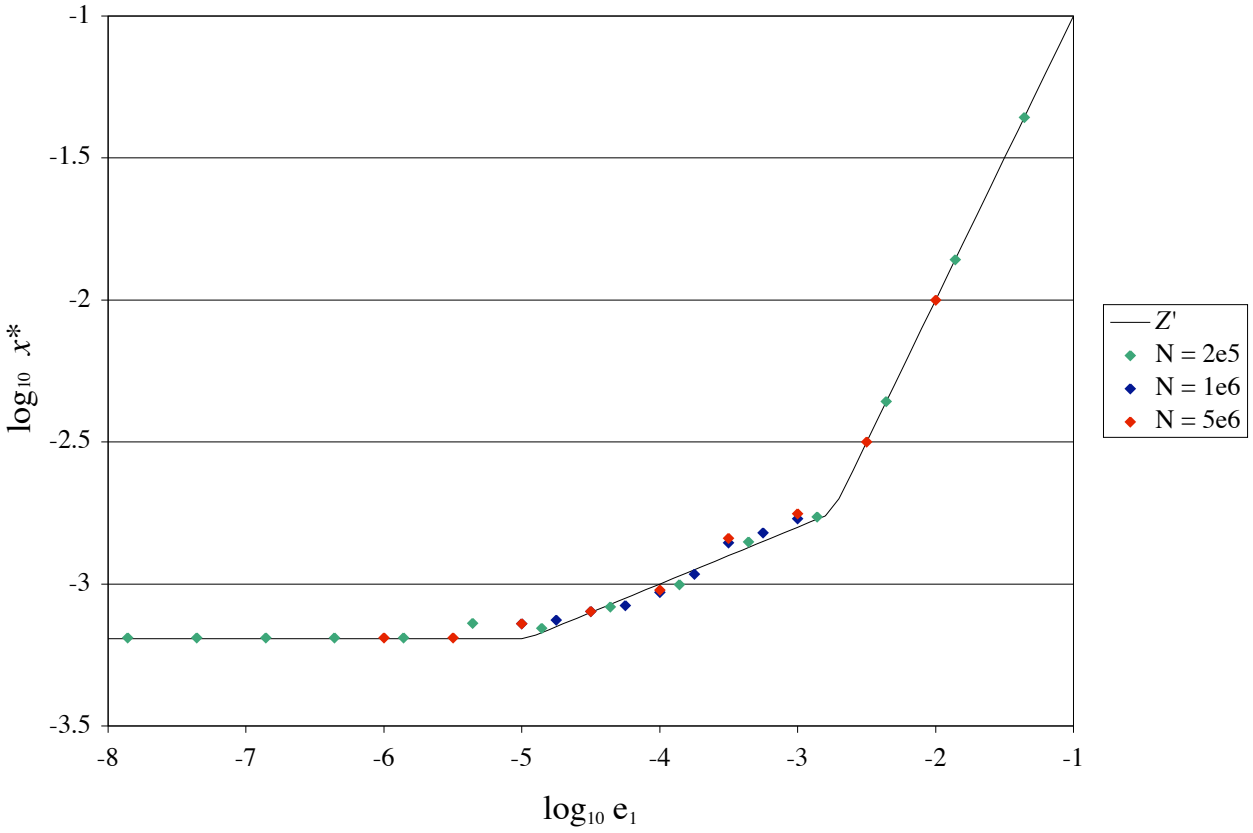

Fig. 6.— Plot of x^* versus e_1, given fixed $\mu = 10^{-12}$; the order 2 Namouni map is applied up to 5×10^6 times; the stability criterion is $e < x_1$. The prediction of the modified indicator Z' is plotted for comparison.

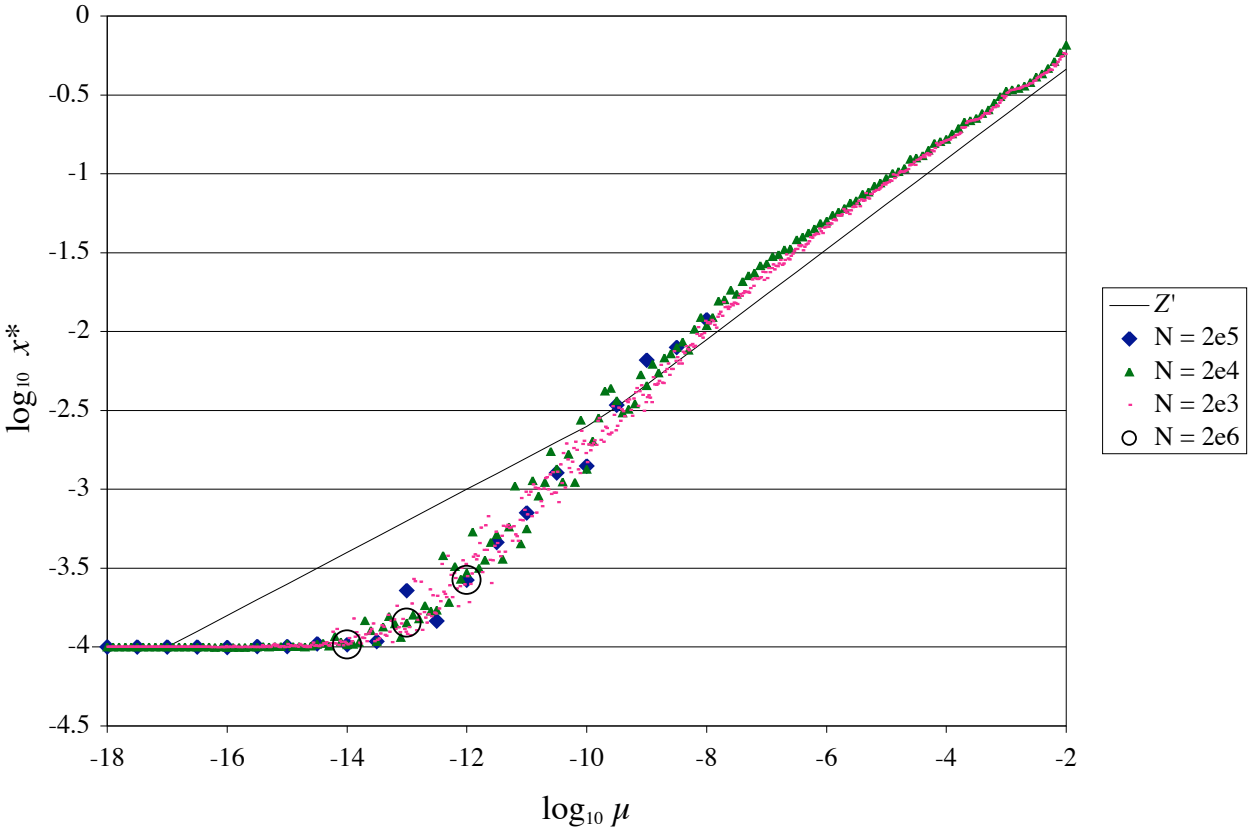

Fig. 7.— Plot of x^* versus μ, given fixed $e_1 = 10^{-4}$; the order 1 Namouni map is applied up to 2×10^6 times; the stability criterion is $e < x_1$. The prediction of the modified indicator Z' is plotted for comparison.

Although the 1/5 law is verified, we are left with a puzzle. Why do the order 1 and order 2 encounter maps differ so widely in their assignments of x^* in the moderate eccentricity regime? Our heuristic derivation of Z involves only the lowest-order contributions in e. It is therefore surprising that the map which includes exactly those contributions fails to detect a chaotic boundary consistent with Z. We suspect that a solution to this puzzle will require a more detailed understanding of the mechanism by which chaos appears.

We thank David Nesvorný for prompting us to make good plots; Yoram Lithwick for pointing out the existence of an intermediate regime of eccentricity; and Eugene Chiang for three years of providing sound advice and interesting problems, including this one.

Also, he pretended not to notice when I stole his UNIX book. Now that's class.

REFERENCES

Chirikov, B.V. 1979, Phys. Rep., 52, 263

Duncan, M., Quinn, T., & Tremaine, S. 1989, Icarus, 82, 402

Lecar, M., Franklin, F., Holman, M., & Murray, N. 2001, ARA&A, 39, 581

Murray, C.D., & Dermott, D.F. 1999, Solar System Dynamics (Cambridge: Cambridge UP)

Namouni, F., Luciani, J.F., Tabachnik, S., & Pellat, R. 1996, A&A, 313, 979

Wisdom, J. 1980, AJ, 85, 1122